Supporting Information

Schünke et al. 10.1073/pnas.1015890108

SI Materials and Methods

NMR Sample Preparation. MloK1 CNBD was expressed as a fusion protein with glutathione S-transferase. Details of cloning, expression of [*U*-^{15}N, ^{13}C] or [*U*-^{15}N]-isotopically labeled recombinant CNBD protein, and cell lysis were described previously (1, 2). After cell lysis soluble and insoluble fractions were separated by centrifugation (50,000 × *g* for 30 min at 4 °C). The supernatant was passed over a glutathione-Sepharose 4B column (30 ml bed volume) equilibrated with cold 1 × PBS buffer (pH 7.4). After the supernatant has been applied, the column was washed with 10 column volumes of cold 1 × PBS binding buffer and about 8 liter washing buffer (50 mM MES, pH 6.5, 100 μM EDTA, 50 mM NaCl) overnight. Furthermore the column was washed with 1 × PBS buffer followed by incubation with thrombin for cleavage of the CNBD domain from the GST tag. Thrombin cleavage yielded the isolated cyclic nucleotide binding domain (Q216 to A355) with additional glycine and serine residues at the N terminus. Cleaved CNBD protein was eluted with two and a half column volumes of 1 × PBS buffer. Cleavage and final purity of CNBD protein after affinity chromatography were evaluated by SDS/PAGE analysis. The buffer was immediately exchanged to buffer A (10 mM MES, pH 6, 100 μM EDTA) on a HiPrep 26/10 desalting column mounted on an Äkta purifier system (GE Healthcare). The desalting step was monitored at 280 nm and 260 nm. Performance of the desalting step was observed by measuring the conductivity. Subsequently ion-exchange chromatography was used to separate both domains, cAMP-free and cAMP-bound CNBD. A cation-exchange chromatography column Mono S HR 5/5 (GE Healthcare) was used and the absorption was monitored at 260 and 280 nm. Buffer A was used as binding buffer and elution was directed with buffer A supplied with 1 M NaCl (buffer B). cAMP-free and -bound CNBD protein was separately eluted and the respective fractions were pooled. cAMP-free and -bound CNBD were dialyzed against buffer C (10 mM potassium phosphate, pH 7, 100 mM potassium chloride, 100 μM EDTA, 0.02% (w/v) sodium azide) and buffer D (10 mM Tris/HCl, pH 7, 100 mM sodium chloride, 200 μM EDTA, 0.02% (w/v) sodium azide), respectively. CNBD was concentrated with an Amicon stirred system (Ultracel PL-3, 3 kDa molecular weight cutoff, Millipore). During the final concentration steps the buffer was exchanged by four volumes of the respective NMR buffer including 5% (v/v) $^{2}H_2O$ and deuterated Tris (D11, 98%, Cambridge Isotope Laboratories)/HCl. The protein concentration was determined with Bradford assay (BioRad). NMR samples contained 0.5 mM [*U*-^{15}N] or [*U*-^{15}N, ^{13}C] labeled CNBD in aqueous solution.

NMR Spectroscopy. Nuclear Overhauser Effect (NOE) distance constraints for structure calculations were derived from three-dimensional (^{1}H-^{1}H-^{15}N)-NOESY-HSQC (3) (120 ms mixing time), aliphatic (^{1}H-^{13}C-^{1}H)-HSQC-NOESY (100 ms mixing time), aromatic (^{1}H-^{13}C-^{1}H)-HSQC-NOESY (4) (140 ms mixing time) and two-dimensional aromatic (^{1}H-^{13}C-^{1}H)-HSQC-NOESY (100 ms mixing time) experiments.

For the characterization of overall and internal motions, ^{15}N longitudinal (R_1) and transverse (R_2) relaxation rates, together with the steady-state {^{1}H}-^{15}N-NOE, were recorded at 298 K on a [*U*-^{15}N] labeled protein sample using standard methods at 600 MHz and 800 MHz proton frequency. Peak integral values were obtained by fitting signals to an adjustable "peak model" shape using the program CARA (5). A superposition of Lorentz and Gauss functions was employed and adjusted manually and independently for both spectral dimensions. For ^{15}N R_1 measurement relaxation delay values of 11, 65, 141, 249, 380, 542, 758, and 1192 ms were applied. For R_2 delays of 10, 30, 50, 70, 90, 110, and 150 ms were used. Data of R_1 and R_2 relaxation experiments were fitted to a mono-exponential decay using the program CurveFit (A.G. Palmer, Columbia University). The correlation time was determined for an isotropic tumbling model using the TENSOR2 (6) package. {^{1}H}-^{15}N-NOE-TROSY spectra (7–9) were acquired with 2.5 s proton saturation.

Proton-deuterium exchange experiments were performed at 298 K. Slowly exchanging amide protons were identified by sequentially recording a set of two-dimensional SOFAST (^{15}N-^{1}H)-HMQC (10) spectra using 0.5 mM [*U*-^{15}N] labeled MloK1 CNBD samples, either in the absence or presence of cAMP, which were lyophilized and resolved in deuterium oxide. The first (^{15}N-^{1}H)-HSQC data points were obtained after a delay of roughly 5 minutes, the last spectrum was recorded after 14 hours for the cAMP-free and 24 hours for the cAMP-bound CNBD. Total measuring time of each experiment was 10.83 and 6.67 minutes for the cAMP-free and -bound MloK1 CNBD, respectively. Relative cross-peak intensities were extracted and fitted using a mono-exponential decay to determine the exchange rate (k_{ex}).

Titration experiments were carried out to a 0.2 mM [*U*-^{15}N] labeled unliganded MloK1 CNBD sample by stepwise addition of small aliquots of concentrated cAMP stock solutions (Sigma-Aldrich). Eight (^{15}N-^{1}H)-HSQC spectra were recorded with increasing ligand concentrations of 5, 10, 25, 50, 75, 100, 250, and 500 μM cAMP.

Data Evaluation and Structure Calculation. Based on an almost complete assignment of ^{1}H, ^{15}N, and ^{13}C resonances of cAMP-free CNBD, NOE cross peak assignments were obtained by an iterative procedure using a combination of manual and automatic steps. CARA was used to evaluate NOE spectra and to manually assign nearly all of the apparently unambiguous NOE distance constraints. NOE cross-peak intensities were classified as strong, medium and weak, corresponding to upper limit distance constraints of 2.7, 3.8, and 5.5 Å, respectively. Intensities of NOE cross-peaks between protons of known distances were used for calibration. For NOE cross-peaks involving methyl groups upper limit distance constraints of 2.9, 4.0, and 5.7 Å for strong, medium or weak interactions were used. Structure calculations were performed using the program CYANA (11). CYANA runs were performed according to the protocol for simulated annealing with 100 randomly generated starting conformations, 25,000 steps torsion angle dynamics and subsequent 2,000 conjugate gradients minimization steps. Using only manually assigned NOE cross-peaks an initial fold of the protein was calculated. Additional NOE cross-peaks were automatically assigned in an iterative approach using ATNOS/CANDID (12, 13) algorithms in combination with CYANA, giving the resonance assignments, all manually assigned NOE cross-peaks and all three-dimensional NOESY spectra as input. The standard protocol with seven cycles of peak picking, cross-peak assignment, and subsequent structure calculation with CYANA was applied. In the final step dihedral angle restraints for backbone Φ and Ψ angles were included that were derived from H^{α}, C^{α}, C^{β}, C', and N chemical shifts using the pro-

gram TALOS (14). For further refinement CYANA runs were performed according to the protocol for simulated annealing with 100 randomly generated starting conformations, 35,000 steps torsion angle dynamics and subsequent 2,000 conjugate gradients minimization steps. A final bundle of 15 NMR structures with the lowest CYANA target function that did not show any distance constraint violations of more than 0.019 nm were used for further analysis.

1. Schünke S, Stoldt M, Novak K, Kaupp UB, Willbold D (2009) Solution structure of the *Mesorhizobium loti* K1 channel cyclic nucleotide-binding domain in complex with cAMP. *EMBO Rep* 10:729–735.
2. Schünke S, Novak K, Stoldt M, Kaupp UB, Willbold D (2007) Resonance assignment of the cyclic nucleotide binding domain from a cyclic nucleotide-gated K^+ channel in complex with cAMP. *Biomol NMR Assign* 1:179–181.
3. Zuiderweg ERP, Fesik SW (1989) Heteronuclear 3-dimensional NMR-spectroscopy of the inflammatory protein C5A. *Biochemistry* 28:2387–2391.
4. Norwood TJ, Boyd J, Heritage JE, Soffe N, Campbell ID (1990) Comparison of techniques for ^{1}H-detected heteronuclear ^{1}H-^{15}N spectroscopy. *J Magn Reson* 87:488–501.
5. Keller R (2004) *The Computer Aided Resonance Assignment Tutorial* (Cantina, Zurich).
6. Dosset P, Hus JC, Blackledge M, Marion D (2000) Efficient analysis of macromolecular rotational diffusion from heteronuclear relaxation data. *J Biomol NMR* 16:23–28.
7. Farrow NA, et al. (1994) Backbone dynamics of a free and a phosphopeptide-complexed Src homology 2 domain studied by ^{15}N NMR relaxation. *Biochemistry* 33:5984–6003.
8. Pervushin K, Riek R, Wider G, Wüthrich K (1997) Attenuated T2 relaxation by mutual cancellation of dipole-dipole coupling and chemical shift anisotropy indicates an avenue to NMR structures of very large biological macromolecules in solution. *Proc Natl Acad Sci USA* 94:12366–12371.
9. Zhu G, Xia Y, Nicholson LK, Sze KH (2000) Protein dynamics measurements by TROSY-based NMR experiments. *J Magn Reson* 143:423–426.
10. Schanda P, Brutscher B (2005) Very fast two-dimensional NMR spectroscopy for real-time investigation of dynamic events in proteins on the time scale of seconds. *J Am Chem Soc* 127:8014–8015.
11. Güntert P, Mumenthaler C, Wüthrich K (1997) Torsion angle dynamics for NMR structure calculation with the new program DYANA. *J Mol Biol* 273:283–298.
12. Herrmann T, Güntert P, Wüthrich K (2002) Protein NMR structure determination with automated NOE-identification in the NOESY spectra using the new software ATNOS. *J Biomol NMR* 24:171–189.
13. Herrmann T, Güntert P, Wüthrich K (2002) Protein NMR structure determination with automated NOE assignment using the new software CANDID and the torsion angle dynamics algorithm DYANA. *J Mol Biol* 319:209–227.
14. Cornilescu G, Delaglio F, Bax A (1999) Protein backbone angle restraints from searching a database for chemical shift and sequence homology. *J Biomol NMR* 13:289–302.
15. Shen Y, Delaglio F, Cornilescu G, Bax A (2009) TALOS+: A hybrid method for predicting protein backbone torsion angles from NMR chemical shifts. *J Biomol NMR* 44:213–223.

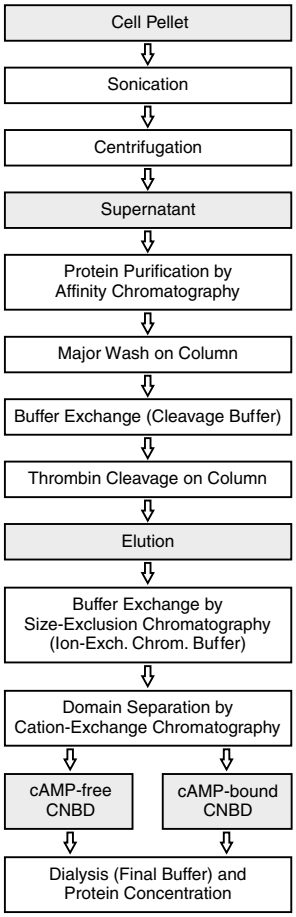

Fig. S1. Overview of the protein purification and separation protocol of cAMP-free and cAMP-bound MloK1 CNBD.

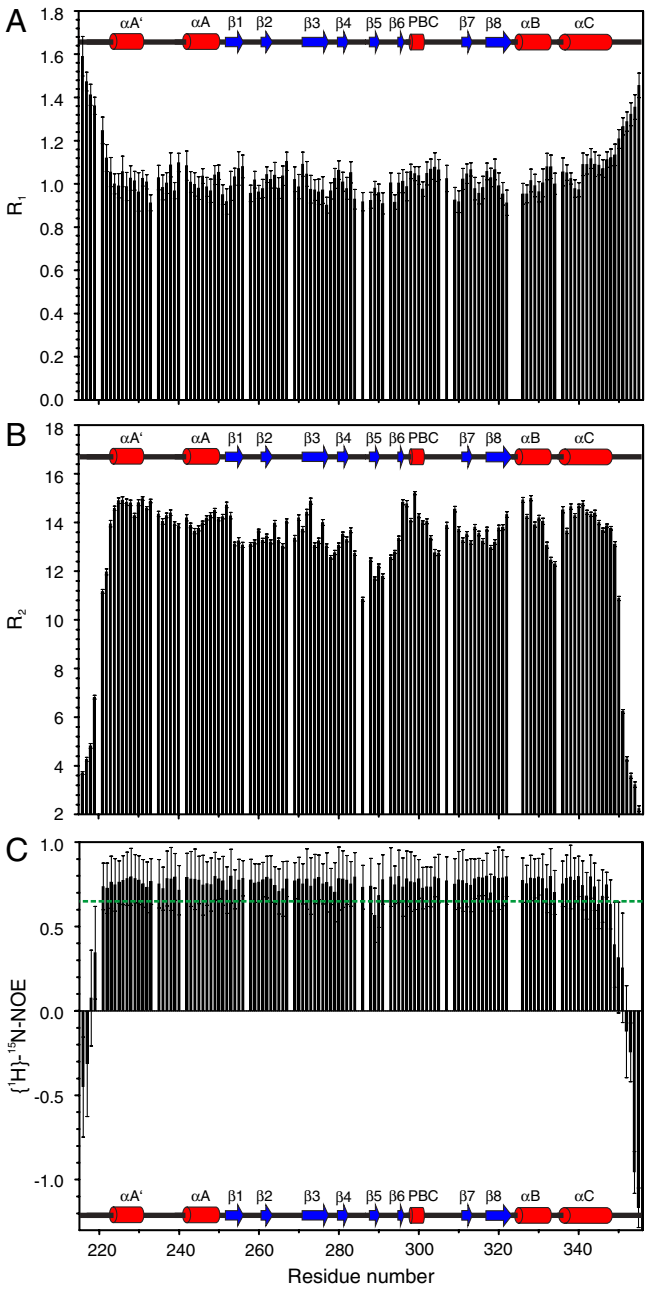

Fig. S2. Experimental values of ^{15}N longitudinal (R_1) and transverse (R_2) relaxation rates for cAMP-free CNBD with respect to the protein sequence: (*A*) R_1 (s^{-1}); (*B*) R_2 (s^{-1}); and (*C*) steady-state heteronuclear $\{^1H\}$-^{15}N-NOE values of amide resonances at 298 K, 14.1 T and 18.8 T. Residues for which no results are shown correspond to prolines and residues R220, S308, H323, S324, and A325. For residues with $\{^1H\}$-^{15}N-NOE values greater than 0.65 (green dashed line), an isotropic rotational correlation time of 8.4 ns at 298 K was derived. Secondary structure elements are shown in each panel (blue arrows indicate β strand and red cylinders indicate α helical conformation).

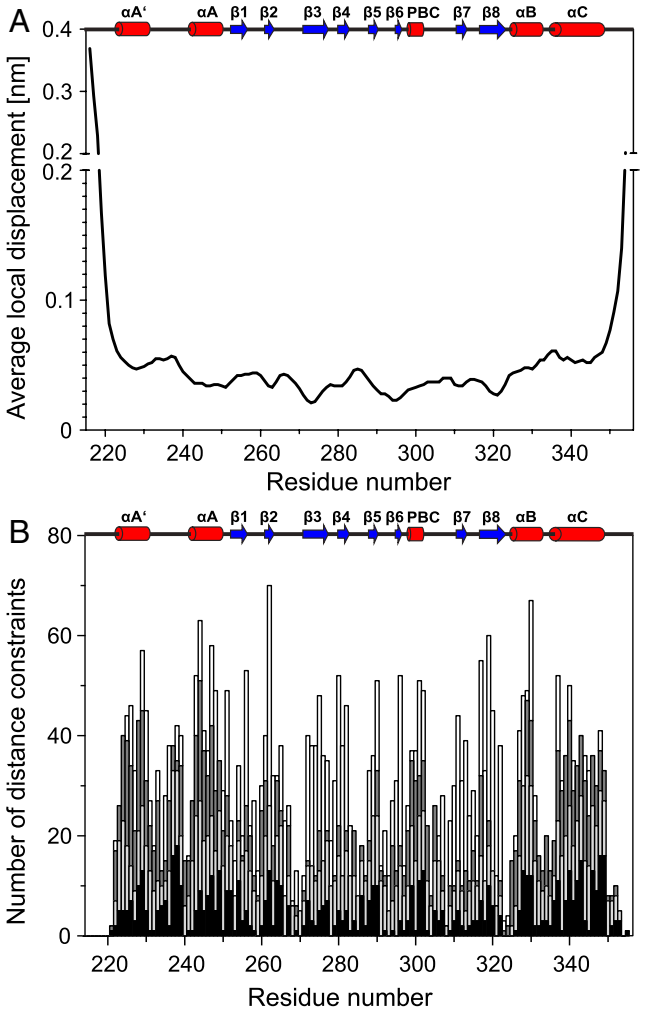

Fig. S3. Precision of local conformation and number of distance constraints per residue for the resulting 15 NMR structures of cAMP-free CNBD with the lowest CYANA target function. (*A*) Average local displacement values among the 15 calculated solution structures. For each three-residue segment the local root mean squared (rms) deviation of the backbone atoms was calculated and plotted against the residue number of the central residue. (*B*) Number of intraresidual (black), sequential (light gray), medium-range (dark gray), and long-range (white) NOE distance constraints per residue.

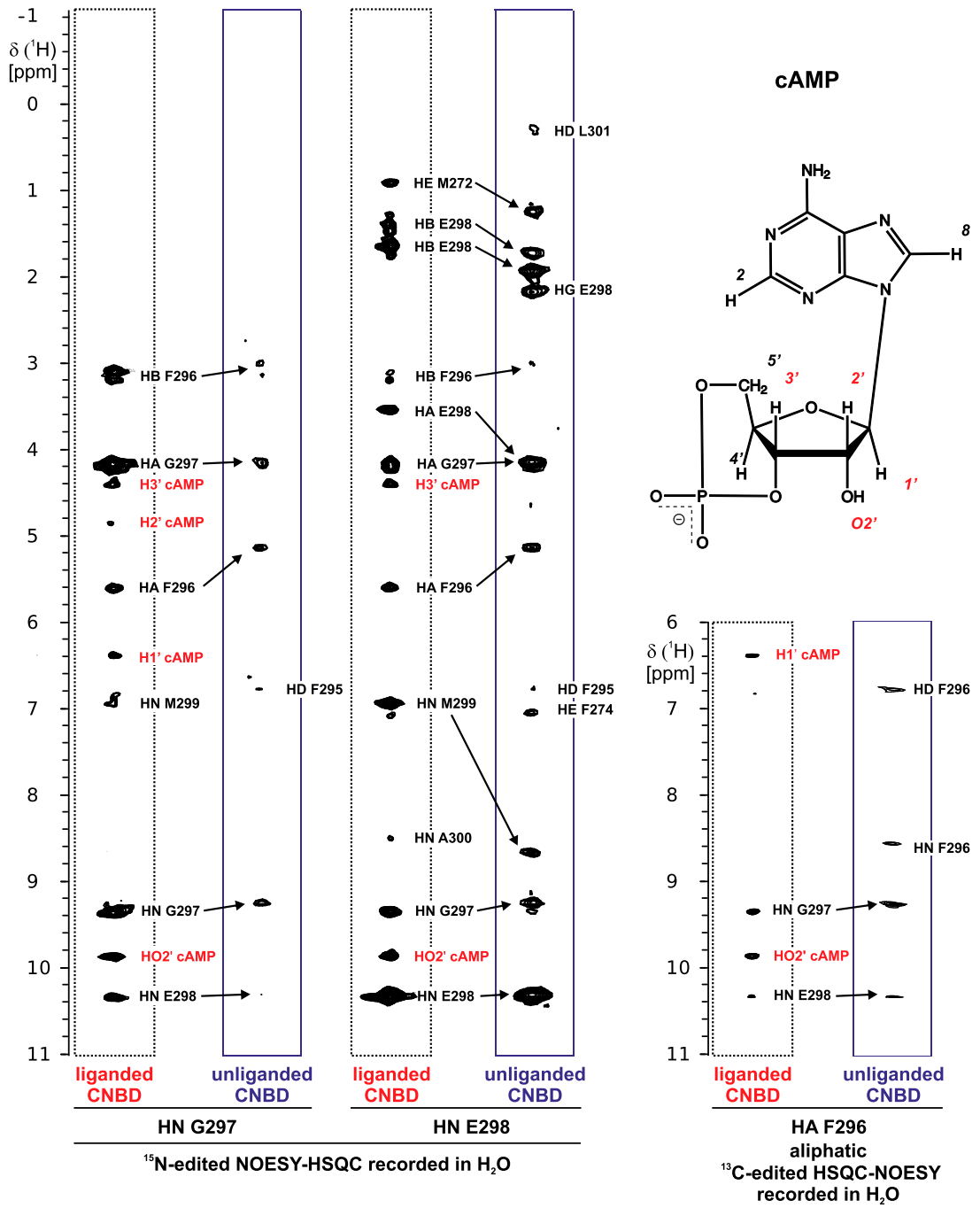

Fig. S4. Comparison of the NOE strips from ^{13}C-edited HSQC-NOESY and ^{15}N-edited NOESY-HSQC spectra of the cAMP-bound and -free CNBD. Shown are strips for the amide protons of G297, E298, and aliphatic alpha proton of F296. Strips of the cAMP-bound CNBD (1) (PDB ID code 2K0G) show intermolecular NOEs between the CNBD and cAMP (red). As compared to the cAMP-bound CNBD, NOEs to the cAMP molecule (red) are absent in all cAMP-free strips (blue). Moreover, the cAMP-free CNBD shows significant changes in chemical shifts and NOE pattern for atoms that are located in the binding site. The respective NOE is characterized by the cAMP proton labeled (scheme in the upper right corner) and CNBD proton labeled to the right of each cross resonance within the respective stripe.

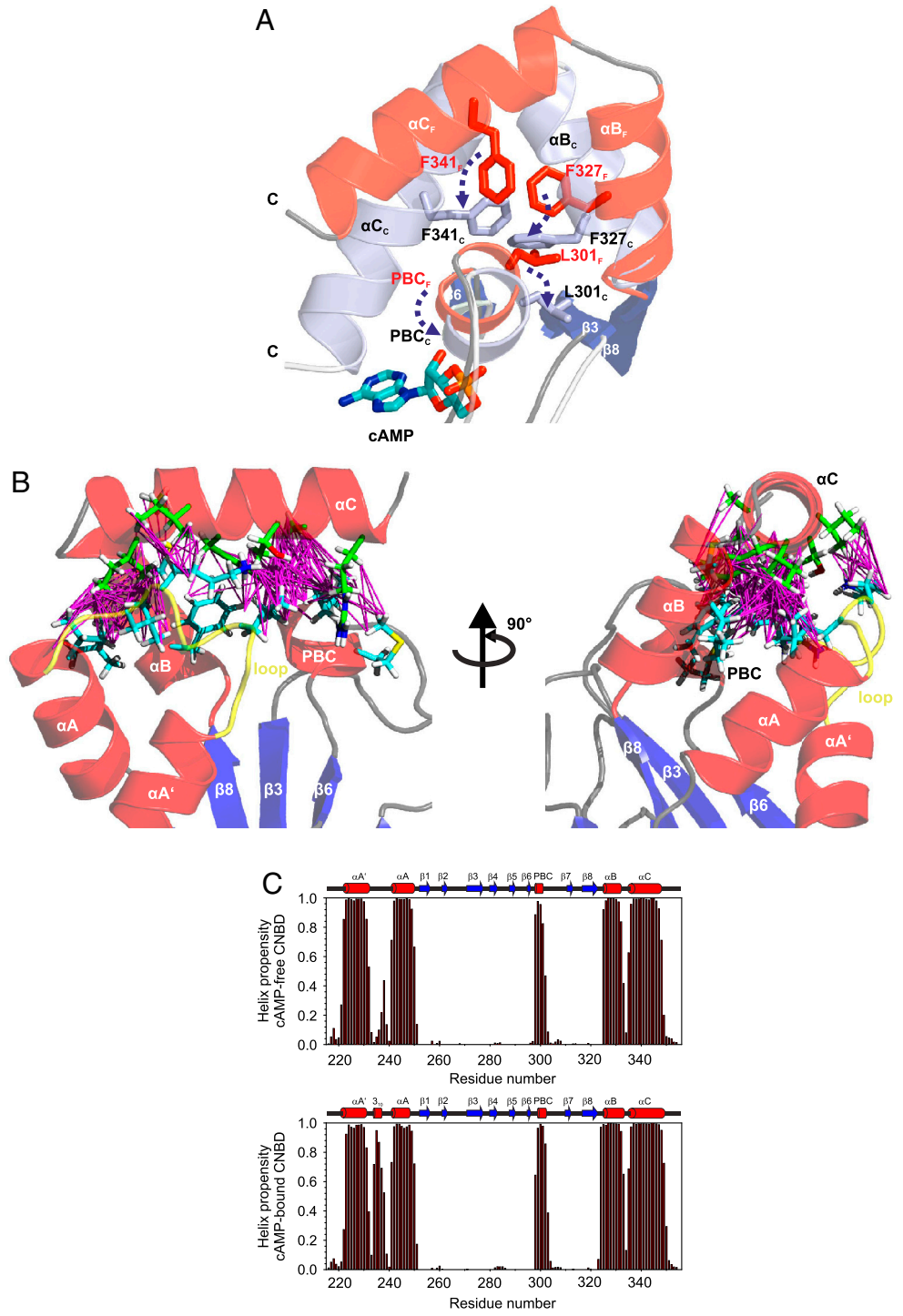

Fig. S5. Comparison of the helical portion of cAMP-free and -bound wild-type MloK1 CNBD. (*A*) A focused view into the reorientation of the C-terminal helical portion. The cAMP-free (red) and -bound (white) CNBD were superimposed. Reorientation of αB and αC helix is induced by binding of cAMP to the PBC helix region. In the cAMP-free state, residue L301 in the PBC helix occupies the space that is filled by F327 in αB helix in the cAMP-bound state, and movement of F327 would clash into L301. Binding of cAMP attracts the PBC, repositions L301, and allows that the resulting gap can be filled by F327. Residue F327 in αB is directly coupled to F341 in αC via hydrophobic interactions and repositioning of F327 leads to the repositioning of F341. Repositioning of the respective residues is shown by arrows. (*B*) Representation of all 48 long-range NOE-derived distances involving residues of helix αC. Two different views are given. (*C*) Helical propensities of cAMP-free (upper) and -bound (lower) CNBD as derived from C^{α}, C^{β}, C′, HA, H_N, and N chemical shifts using the program TALOS+ (15). β strands in both structures are shown in blue. Secondary structure elements are shown and labeled (label "$_C$" stands for "cAMP-bound state"; label "$_F$" stands for "cAMP-free state").

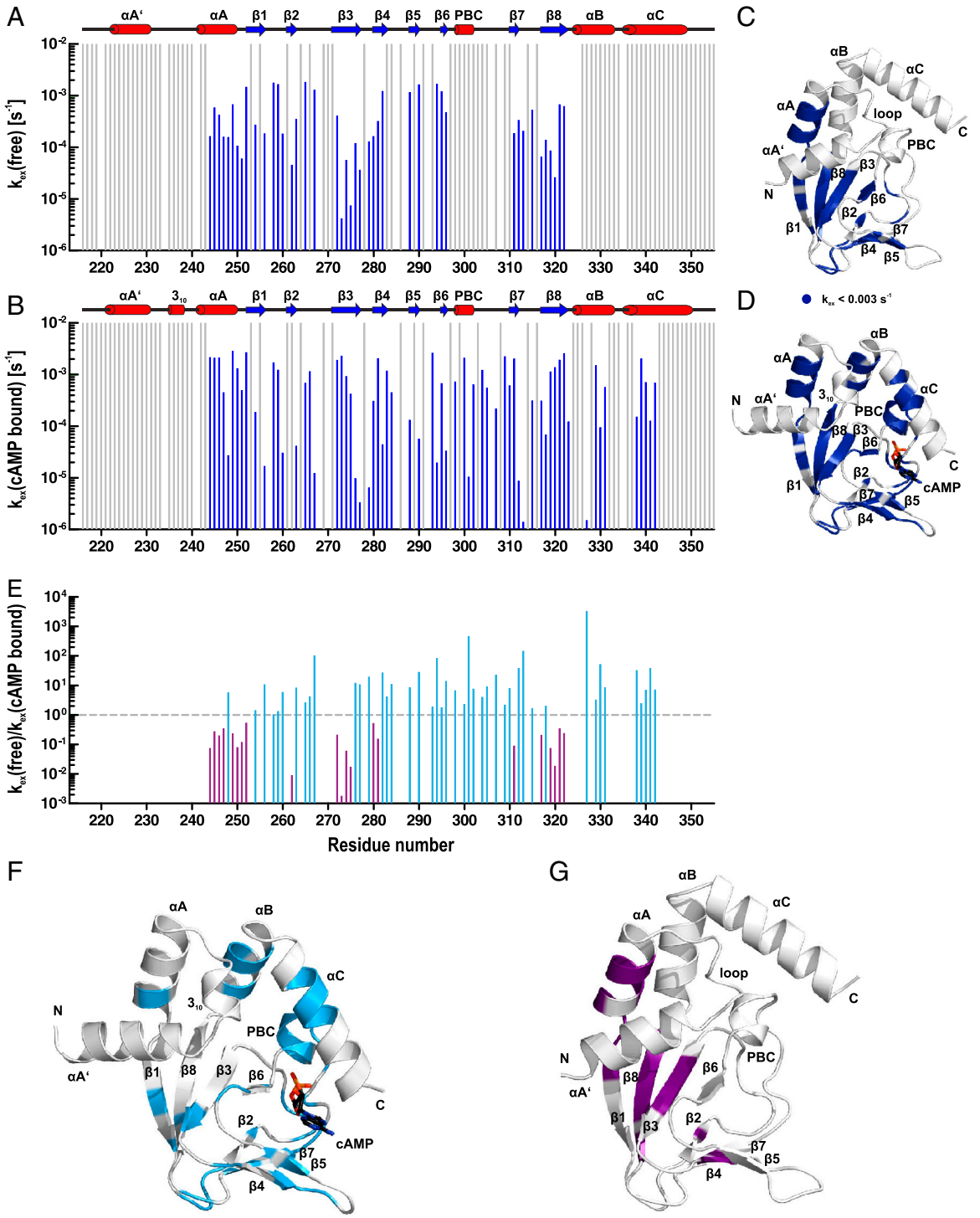

Fig. S6. Proton-deuterium exchange in the absence and presence of cAMP. Exchange rates (k_{ex}) of the respective CNBD residues in the absence (*A*) or presence (*B*) of cAMP. Residues for which the proton–deuterium exchange reaction was almost completed after 300 s are shown in gray. Secondary structure elements are shown on top of each panel. Ribbon representation of the cAMP-free (*C*) and cAMP-bound (*D*) CNBD. Residues with slower exchange rates are shown in blue. (*E*) Ratio of exchange rates of the cAMP-free and -bound CNBD. Residues with values greater than one (gray dotted line) show an enhanced protection in the cAMP-bound state compared to cAMP-free state. Residues with values less than one show an enhanced protection in the cAMP-free compared to the cAMP-bound state. Protection factors of residues for which the exchange in the absence or presence of cAMP was almost complete after 300 s are also shown. In these cases, a value for k_{ex} of 0.005 s^{-1} was assumed to calculate the underestimated ratio. Residues with an elevated protection against proton–deuterium exchange were mapped onto the solution structures of the cAMP-bound (*F*) and cAMP-free (*G*) CNBD.

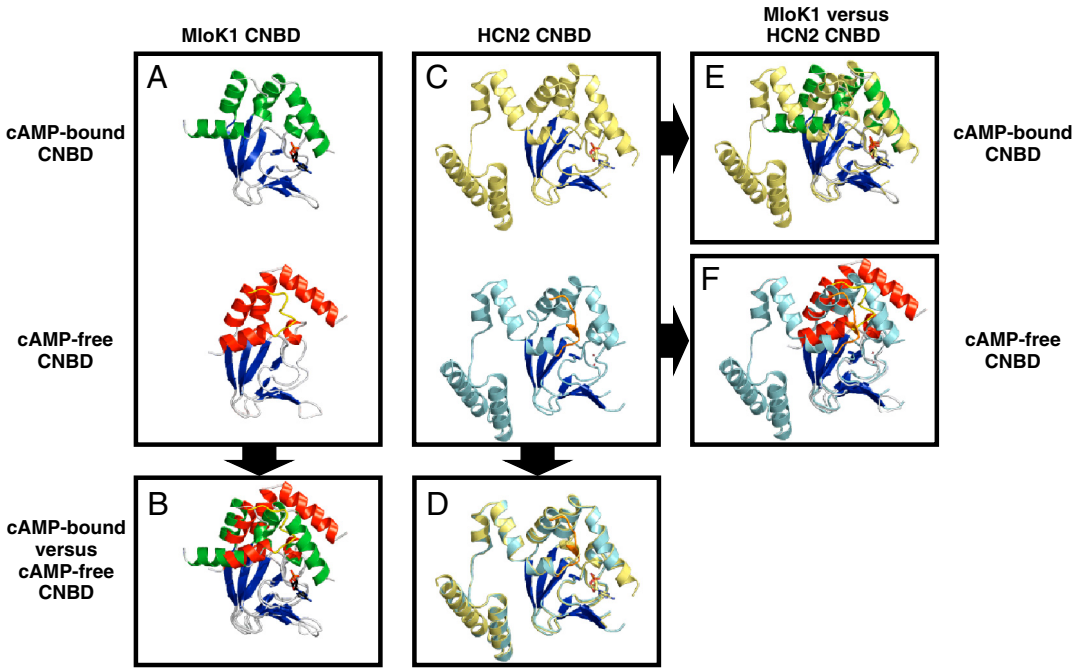

Fig. S7. Comparison of cAMP-bound and -free MloK1 CNBD solution structures and monomers of eukaryotic HCN2 CNBD crystal structures. The solution structure of the cAMP-bound and -free wild-type MloK1 CNBD (*A*) is superimposed onto each other (*B*). The cAMP-bound and -free CNBD structure of the HCN2 channel (*C*) is superimposed onto each other (*D*). The cAMP-bound and -free MloK1 CNBD solution structure is superimposed onto the cAMP-bound and -free CNBD crystal structure of the HCN2 channel (*E* and *F*). The CNBDs were taken from PDB ID codes 2K0G (MloK1 CNBD holo state (1), helices are shown in green), 1Q43 (HCN2 CNBD holo state (2), helices are shown in light yellow), 2KXL (MloK1 CNBD apo state, helices are shown in red and loop region in yellow), and 3FFQ (HCN2 CNBD apo state (3), helices are shown in light blue and loop region in orange). β strands are shown in blue and cAMP in stick model. The least-square superposition of the structures was done using the backbone atoms of the β roll forming strands. MloK1 CNBD backbone atoms of the amino- and carboxy-terminal ends (residues Q216-R220 and A351-A355) are not shown.

1 Schünke S, Stoldt M, Novak K, Kaupp UB, Willbold D (2009) Solution structure of the *Mesorhizobium loti* K1 channel cyclic nucleotide-binding domain in complex with cAMP. *EMBO Rep* 10:729–735.

2 Zagotta WN, et al. (2003) Structural basis for modulation and agonist specificity of HCN pacemaker channels. *Nature* 425:200–205.

3 Taraska JW, Puljung MC, Olivier NB, Flynn GE, Zagotta WN (2009) Mapping the structure and conformational movements of proteins with transition metal ion FRET. *Nat Methods* 6:532–537.

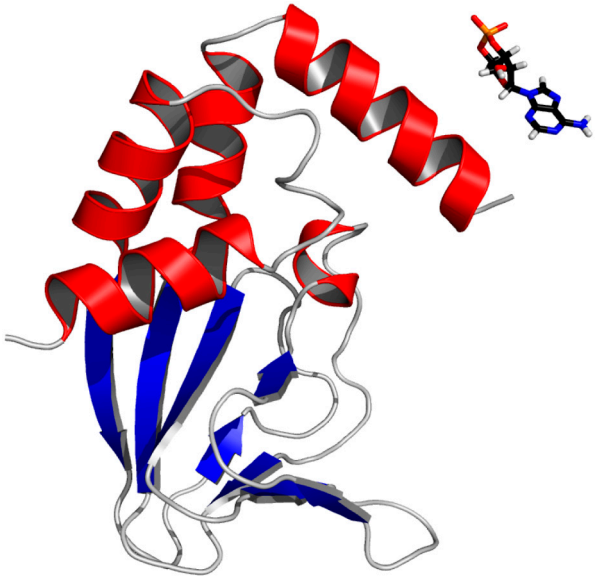

Movie S1. Structure comparison of cAMP-free and -bound wild-type MloK1 CNBD—an animation to illustrate the large conformational rearrangement on ligand binding. The CNBD is shown in ribbon representation and the cAMP molecule is shown as stick model.

Movie S1 (GIF)

Table S1. NMR constraints and structural statistics for the resulting 15 NMR structures of cAMP-free CNBD

Number of experimental NMR restraints:	
Total number of assigned NOEs	2,380
Intraresidue ($\|i-j\|=0$)	665
Interresidue sequential ($\|i-j\|=1$)	627
Interresidue medium-range ($1<\|i-j\|\leq 5$)	456
Interresidue long-range ($\|i-j\|>5$)	632
Average number of NOE constraints per residue	17
Dihedral ϕ and ψ angle constraints from TALOS*	254
CYANA structural statistics†:	
RMS deviations (nm) to mean structure‡:	
Backbone heavy atoms	0.037 ± 0.007
All heavy atoms	0.070 ± 0.007
CYANA target function (nm^2)	0.058 ± 0.005
NOE distance constraints, sum (nm)	0.28 ± 0.040
NOE distance constraints, max (nm)	0.017 ± 0.002
Dihedral angle constraints, max (°)	3.37 ± 0.460
Φ, Ψ angles consistent with Ramachandran plot§:	
Most favored regions (%)	89.9
Allowed regions (%)	99.2
Generously allowed regions (%)	100
Disallowed regions (%)	0

*Derived from C^{α}, C^{β}, C′, N and H^{α} chemical shifts for 127 high confidence predictions found by TALOS using the calculated range of ±10°.

†Average value ± standard deviation.

‡Superposition made for all heavy atoms (except N- and C-terminal residues Q216-G221 and R349-A355).

§Ramachandran analysis was determined using PROCHECK-NMR.